# Fizeau interferometer with spherical reference and CGH correction for measuring large convex aspheres

M. B. Dubin, P. Su and J. H. Burge
College of Optical Sciences, The University of Arizona
1630 E. University Blvd., Tucson, AZ USA 85721

## ABSTRACT

Large, convex surfaces, such as secondary mirrors, have presented challenging metrology problems for many years. Over the years, new metrology approaches have been developed to keep pace with the ever changing definition of "large". The latest class of large secondary mirrors requires a new approach that is practical, scalable and can produce low uncertainty measurements. This paper presents a new configuration that uses a computer generated hologram based Fizeau interferometer to make sub-aperture measurements on large secondary mirrors. One of the key features of this system is that all of the surfaces used in the interferometer are spherical. Another key element is the ability to perform simultaneous phase shift interferometry which reduces sensitivity to vibration. An example system that is capable of measuring the Large Synoptic Survey Telescope secondary mirror is presented along with a sensitivity analysis.

**Keywords:** Interferometry, Aspheres, Optical testing, Computer generated holograms

## 1. INTRODUCTION

It is well known that measuring large convex surfaces is difficult because many of the test schemes require auxiliary optics that are slightly, to significantly larger than the optic being tested[1,2,3]. One solution that has been successfully used to test large convex surfaces is a holographic test plate[4]. The problem with this approach is that the definition of large keeps changing. About ten years ago, a large convex surface was 1.7 m in diameter[5]. Since then, designs have progressed for telescopes that will have secondary mirrors that are up to 6 m in diameter[6]. New approaches are required to test these mirrors and the even larger mirrors that are sure to come.

In this paper we present an alternate approach that combines elements of the holographic test plate[4], subaperture Fizeau testing with an aspheric reference[7], and use of a CGH to compensate the Fizeau testing with a spherical reference[8]. This test uses all-spherical surfaces and computer generated holograms to provide accurate subaperture surface measurements. Increasing the size and number of the subapertures allows arbitrarily large surfaces to be measured. Furthermore, we add an element that allows simultaneous phase shifting, providing several simultaneous, phase shifted fringe patterns. This allows "snapshot" measurements to be taken, which greatly reduces the sensitivity to vibration that can hinder systems that use temporal phase shifting (a sequence of measurements with different phase shifts.)

To demonstrate the concept, we have completed a preliminary design and sensitivity analysis for a test system capable of measuring the Large Synoptic Survey Telescope (LSST) secondary mirror. This is a convex mirror that is 3.4 m in diameter with a 1.8 m central obscuration[9].

## 2. SYSTEM CONCEPT

The LSST secondary is an ellipsoid with 6$^{th}$ and 8$^{th}$ order aspheric terms. The higher order terms and the multi-point support on the rear surface of the mirror make a finite conjugate test impractical. The performance requirements indicate a need for the sampling and accuracy provided by interferometry. We accomplish this with a sub-aperture Fizeau interferometer that uses a spherical, concave reference surface and a CGH for wavefront matching.

mdubin@optics.arizona.edu, phone: 520-626-3723, fax: 520-621-3389

Optical Manufacturing and Testing VIII, edited by James H. Burge, Oliver W. Fähnle, Ray Williamson,
Proc. of SPIE Vol. 7426, 74260S · © 2009 SPIE · CCC code: 0277-786X/09/$18 · doi: 10.1117/12.829053

In the past, CGHs written directly onto a reference surface that is in close proximity to the test surface have proven effective. These were written with a CGH writer that relies on the rotational symmetry of the CGH pattern[10]. This means that a CGH writer with a 3.4 m capacity would be required even if the CGH only had to cover a sub-aperture of the mirror. This capacity does not exist, and developing it would only result in a system that works for the current batch of "large" secondaries, but would be obsolete when even larger surfaces are required.

To solve this problem we propose to use a smaller CGH and image it onto a sub-aperture of the secondary mirror. Because the number of sub-apertures can be traded off with the size of the test system and the time it takes to make a complete measurement, this approach allows for flexibility that can be tailored to the surface being tested and its requirements. This provides the desired growth path for future mirrors. For this design, we used one ring of twelve sub-apertures that are 1.1 m in diameter. Figure 1 shows the layout of the LSST secondary clear aperture and the arrangement of the sub-apertures.

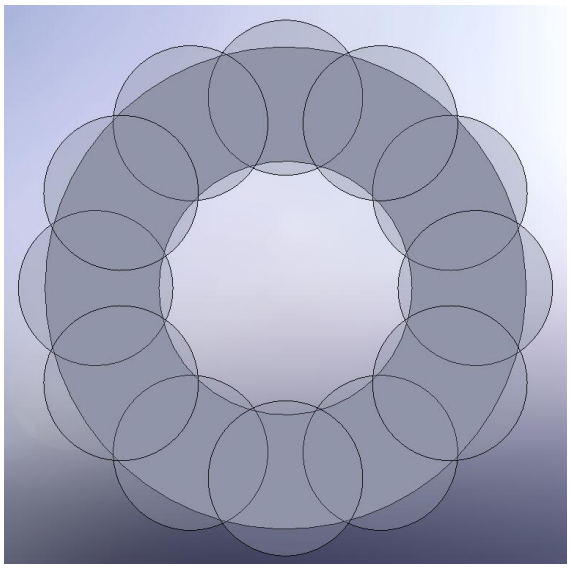

Figure 1. The grey annulus shows the 3.4-m diameter LSST secondary clear aperture. The semi-transparent circles represent the twelve 1.1 m sub-aperture locations.

Figure 2 shows the entire system that is used to measure the secondary mirror. The system is divided into two major sections. The beam launch and imaging sub-system (BLISS) contains the optics shown in the upper right had corner of the figure. They are also shown in the inset. The other section is the test plate cell (TPC) which consists of the illumination lens and the test plate. These are mounted in close proximity to the secondary mirror. The distance from the BLISS to the TPC is approximately 5 m. This means that the BLISS would be mounted in a test tower and the TPC would be mounted on the structure that supports the mirror during polishing. The alignment between the two is set and monitored by including alignment marks on the CGH that are imaged onto cameras on the TPC. Since the alignment marks are fabricated as part of the CGH, their locations with respect to the CGH are known with very low uncertainty. To record the images of these marks, the cameras are positioned on the TPC, and their locations with respect to key data are measured with a laser tracker.

To understand how the system works it is necessary to identify the components and describe each one's purpose. Starting at the source, there is a pair of point sources with orthogonal polarization. This configuration is used to allow for instantaneous phase shifting, which makes the system insensitive to vibration and air turbulence. The next element after the source is the condenser lens. The condenser lens turns a diverging wavefront into a converging one. At a fundamental level, it is not required, but it serves the purpose of minimizing the size of the projection lens. This will be addressed later in the discussion on the sensitivities. After the condenser lens is the CGH. There are actually two CGH patterns that are superimposed on the same substrate. The first CGH, the common CGH, is used to correct the aberrations in the reference arm of the system. The complexity and tolerances that would be required to build a reference arm that is good enough to use without a CGH make it impractical. This feature is part of what enables the used of a spherical reference surface. While it is not apparent from this figure, the common CGH has a linear carrier frequency that spreads the orders out in one direction. The other CGH, the test CGH, is used to correct the wavefront that reflects off of the secondary mirror so that a null fringe is obtained for a perfect system.

The test CGH and common CGH provide different functions. Both the test and reference wavefront use the first order of diffraction from the common CGH, thus any error in this is common to both and does not affect the measurement. We use two different orders of diffraction from the test CGH. The zero order is used for the reference wavefront, reflected

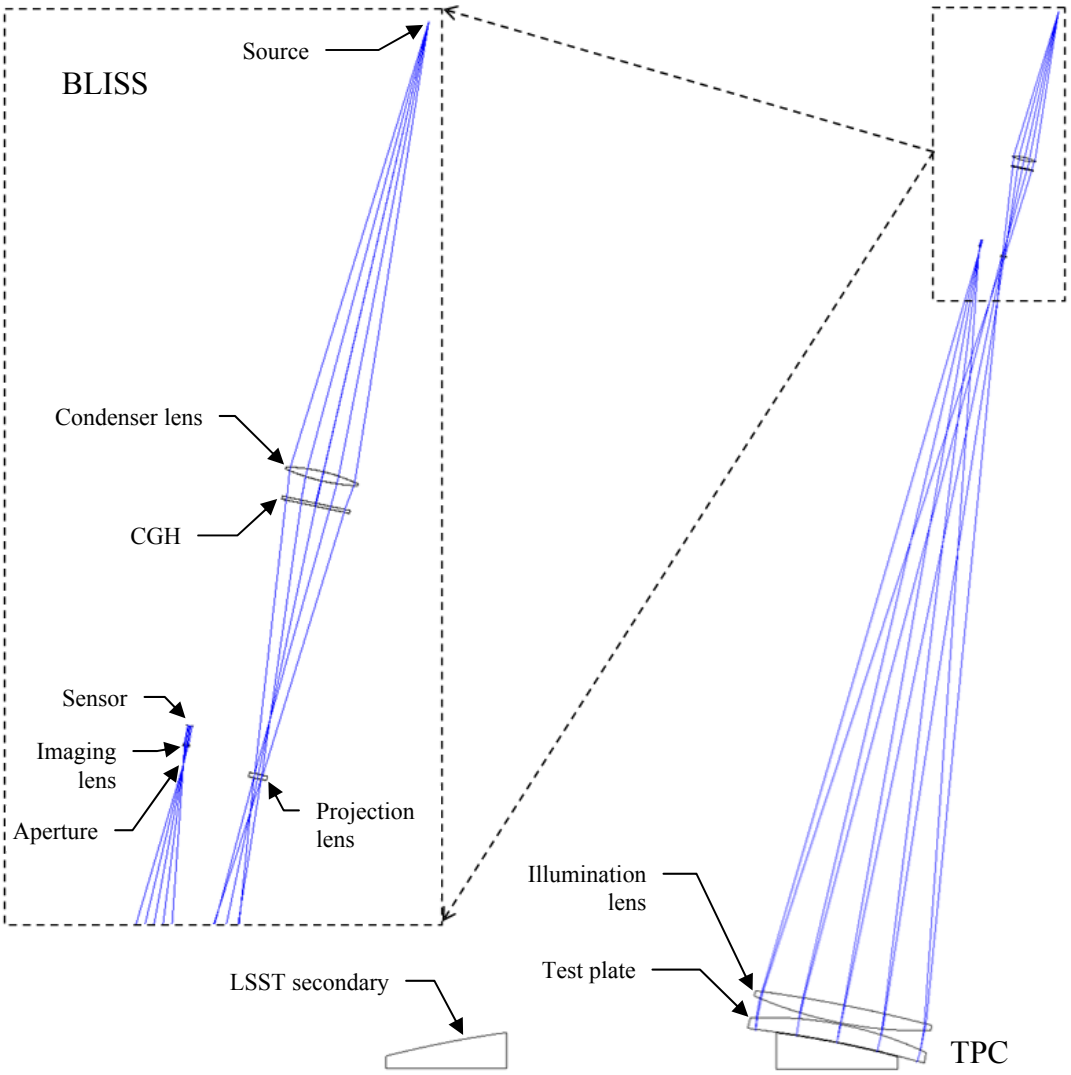


Figure 2. Cross section of interferometer for measuring LSST secondary mirror.

from the spherical test plate. The first order of diffraction from the test CGH compensates the aspheric departure of the test wavefront as it is reflected from the mirror under test. The orientation of the carrier for the two CGHs is orthogonal, allowing complete isolation of the desired orders of diffraction with an aperture in the imaging system.

After the CGHs, the next element is the projection lens. The function of the projection lens is to image the CGH onto the secondary mirror. The reason why this is done is to minimize the amount of shear or shift between the test and reference beams on the condenser lens and the CGH. One thing that is obvious in figure 2 is that the projection lens is well within the caustic formed by the condenser lens and the CGHs. The reasons for this will be discussed in the following section on sensitivities.

Up to this point, the optics that have been covered make up the "beam launch" portion of the BLISS. At the highest level, this sub-system can be thought of as a slide projector using Köhler illumination. The point sources are equivalent to the light bulb, the condenser lens is exactly that, the CGH is the "film", and the projection lens images the "film" onto the secondary mirror which is the "screen." There are some details, however, like the wavefront error in the condenser

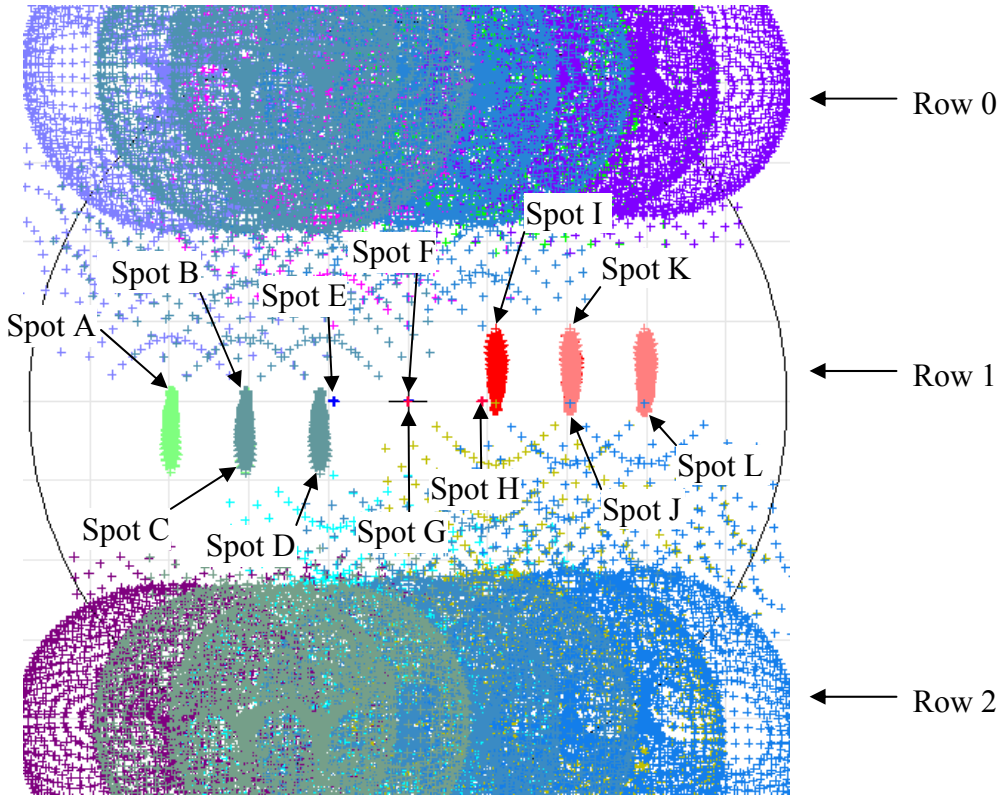


Figure 3. Spot diagrams in the aperture plane. The partially obscured circle is 40 mm in diameter. Row 0 is the $0^{th}$ order from the common CGH, row 1 is the $1^{st}$ order and row 2 is the $2^{nd}$ order. The different diffracted orders in row 1 are identified in table 1.

lens, that are not important in a slide projector but matter in this system. Regardless of the differences, the fundamental purpose of the beam launcher is to project the CGH onto the secondary mirror.

The next two elements make up the test plate cell: the illumination lens and test plate. The illumination lens and the convex surface of the test plate turn a diverging wavefront from the BLISS into a converging one that matches the convex curvature of the mirror under test. The other key feature of these optics is the reference surface. The concave, spherical surface of the test plate acts as the reference creating a Fizeau cavity. The desire is to get the test plate as close as possible to the secondary mirror to reduce sensitivity to errors. For this design, the separation was chosen to be 5 mm. This makes the large optics in the test nearly common path. What is also significant about the reference surface is that it is spherical. Not only does this reduce the fabrication cost, but it can be easily tested with a standard interferometer. This allows for a low uncertainty calibration of the reference surface.

The final large optic is the mirror being tested. The purpose of this mirror in the test should be self evident. What is significant is that this test is designed so that it can be performed while the mirror is on the polishing machine. This means that the mirror does not have to be moved when it is tested. Minimizing the number of times that a mirror of this size is moved reduces cost, schedule, and, most importantly, risk.

Following the light from the large optics, the final sub-system is the imaging system. The first item in the imaging system is the aperture. The aperture is required to block the unwanted diffracted orders from the CGH. The carrier frequencies in the CGHs are chosen so that the orders are well separated and they can be easily blocked. Figure 3 shows the spot diagrams in the aperture plane. In this plane, the edge of a 2.5 mm diameter aperture would be equidistant from the two desired orders and the closest ray from an undesired order. In order for all of the rays to be passed by the

| Spot | Diffracted order | Surface | Source |
|---|---|---|---|
| A | 2 | secondary | 1 |
| B | 2 | secondary | 2 |
| C | 1 | reference | 1 |
| D | 1 | reference | 2 |
| E | 1 | secondary | 1 |
| F | 1 | secondary | 2 |
| G | 0 | reference | 1 |
| H | 0 | reference | 2 |
| I | 0 | secondary | 1 |
| J | 0 | secondary | 2 |
| K | -1 | reference | 1 |
| L | -1 | reference | 2 |

Table 1. Parameters that determine the location and size of each spot in figure 3.

aperture without transmitting any undesired light, the optical system has to have angular errors that are less than 250 μrad. The sensitivity analysis that was performed did not check this, but it is likely that other tolerances will drive the system to be better than this. Ultimately, if this is not the case, the carrier frequencies in the CGH can be increased with very little impact on the overall uncertainty in the system.

It is helpful to look at where the different orders in figure 3 come from. The orders from the common CGH are distributed vertically and the orders from the test CGH are distributed horizontally. All of the orders are shown, but one should keep in mind that the power in each order will depend on the duty cycle of the CGH. There are a total of 36 spots in figure 3. There are two sources, nine diffracted orders are shown, and each reflects off of the reference surface and the secondary mirror. The spots in the $0^{th}$ and $2^{nd}$ order of the common CGH overlap significantly, so it is not practical to identify each spot. It is, however, possible to do this for the $1^{st}$ order. Table 1 identifies the path for each of these spots. Spots F and G are the desired spots, and they are passed by the aperture. It should also be noted that spots B and C as well as spots J and K are nearly identical in shape and overlap. They have the same shape because each has an extra "dose" of asphericity. Spot B is the second order from the test CGH and it reflects off of the secondary. This means that this beam has two times the aspheric wavefront necessary to get a null fringe off of the secondary mirror. Spot C is from the first order of the test CGH so it has the corrections for the secondary in it, but it reflects off of the spherical reference surface. The angle between the test plate and the secondary mirror is set so that the desired spots overlap in the aperture. This angle results in other spots overlapping as well.

The last two optics are the imaging lens and the sensor. The imaging lens is used to image the secondary mirror onto the sensor, and it is also designed so that the light incident on the sensor is nominally telecentric. The imaging lens is truly common path, so it does not need to be a high quality lens. The sensor could be any of the commercially available instantaneous phase sensors which accept two wavefronts with orthogonal polarization and create multiple interferograms with known phase shifts between them[11,12].

## 3. SENSITIVITY ANALYSIS

Tolerance analysis of the 1.1-m test shows that high accuracy can be achieved for the subaperture measurements without requiring overly tight mechanical or optical tolerances. To determine appropriate tolerances, a sensitivity analysis was performed. Each optic was perturbed and the system was aligned by optimizing the adjustable degrees of freedom against the metrics used to determine the alignment. The test and reference wavefronts were fitted to the first 43 standard Zernike terms over the 1.1-m subaperture. A term by term subtraction of the reference wavefront from the test wavefront gives the measurement error for each perturbation. The error terms can be added in quadrature for a given perturbation, or all of the contributions to one Zernike can be added in quadrature to look at what the errors in the whole system will be. The residual error from fitting the Zernike terms for all of the perturbations is 0.7 nm RMS wavefront.

Table 2 shows the perturbations that were used. For this analysis, the local coordinate system of each optic is used. The Y direction is generally in the direction that points towards the center of the secondary mirror. The Z direction is along the local optical axis. What is important to note is that the values in this table are really the uncertainties in the knowledge of the system. Any low order error of modest magnitude can be easily compensated for in the CGH, as long as it is well known. Some of the tolerances are loose enough that they can be met with standard shop practices, while others require a more careful measurement. It is possible to do better in all of the areas without developing new approaches, and we fully expect to do better on some using our standard practices.

To help explain why the listed uncertainties where chosen and what the sensitivities in the system are, it is helpful to look at each element a second time. The source is the first element. It consists of two diffraction limited point sources separated by a fixed distance. If the sources are not where they are designed to be, the primary errors arise from field aberrations. If they are aimed the wrong way, the error will be a mismatch between the light distribution and the entrance pupil of the interferometer. While this is not desirable, it does not cause measurement errors. Because of this, the only errors that were considered were translational ones. The X and Y decenters are small numbers because the source will be aligned to a datum. The alignment approach that would be used can easily detect a 2 μm decenter, so the uncertainties used should be interpreted as the stability of the mount. Also, the spacing is the uncertainty in the distance between the source and the next element. The separation between the two sources is listed in the misc. column. Using a video microscope and a translation stage, it is straightforward to measure this with a 25 μm uncertainty.

The next element is the condenser lens. Because this test is not truly common path, the shear between the test and reference beams at any surface plays a significant role in determining the sensitivities at that surface. For the condenser lens, the shear is a little less than 0.5 mm. This means that errors in the glass and surface that have a spatial frequency of a millimeter or less would strongly couple into the measurement. With good quality glass and a smooth polish, these errors will be negligible. The other sources of error come from the low order fabrication and alignment uncertainties in the lens. None of the uncertainties for the condenser lens listed in table 2 are challenging to meet.

After the condenser lens is the CGH. Clearly the errors in the test CGH pattern will directly couple into the measurement errors. The test CGH has a maximum line spacing that is approximately 30 μm. Based on several CGHs that we have had characterized in the past, the uncertainty in the line position is about 70 nm (2σ). This means that the

| | X decenter (mm) | Y decenter (mm) | Z (spacing) (mm) | X tilt (mrad) | Y tilt (mrad) | clocking (mrad) |
|---|---|---|---|---|---|---|
| **source** | 0.01 | 0.01 | 0.1 | | | 0.3 |
| **condenser lens** | 0.05 | 0.05 | 0.1 | 0.3 | 0.3 | |
| **CGH** | 0.01 | 0.01 | 0.1 | 0.08 | 0.08 | 0.08 |
| **projection lens** | 0.1 | 0.1 | | 0.3 | 0.3 | |
| **illumination lens** | 0.1 | 0.1 | 0.25 | 0.3 | 0.3 | |
| **test plate** | null fringes | null fringes | null fringes | 0.05 (front surface) | 0.05 (front surface) | |
| **BLISS** | 0.1 | 0.1 | 0.1 | | | 0.18 |

| | thickness | power (per surface) | Astigmatism Z5 (waves) | Astigmatism Z6 (waves) | misc |
|---|---|---|---|---|---|
| **source** | | | | | separation: 0.025 mm |
| **condenser lens** | 0.1 | (0.007, 127) | 1 | 1 | |
| **CGH** | 0.1 | | | | |
| **projection lens** | 0.1 | 1/8 wave | 1/16 | 1/16 | index: 0.0001 |
| **illumination lens** | 0.25 | (0.01, 914) | | | |
| **test plate** | 0.25 | (0.01, 914) | | | |

Table 2. Uncertainties used for sensitivity analysis. The test plate will be aligned to null the fringes so there is not a full set of perturbations for it. The power is specified as a sag error. When two numbers are given, the first is the sag uncertainty and the second is the diameter of the spherometer. Otherwise, the sag is measured in waves. Astigmatism is the peak-to-valley transmitted wavefront error for the element.

errors in the CGH pattern will contribute less than 1.5 nm RMS wavefront error to the measurement.

What does matter is the alignment of the image of the CGH on the secondary mirror. If this image is misaligned, there will be shear between the wavefront and the surface being tested. This will result in measurement errors. Because of this, we align the BLISS optics to the CGH. Therefore the only tolerances associated with the CGH are due to stability.

The next element in the system is the projection lens. The shear is greatest at this lens and is about 5 mm. Because of this, high, mid and low spatial frequency errors will all contribute to measurement errors. To complicate matters further, this lens is in the caustic which means that low order errors in the lens will couple in to higher order errors in the data. Based on this, one should expect that this lens will be highly sensitive, and the uncertainties selected show this.

The tradeoff is that all of the things that one could do to try to reduce these sensitivities result in a larger lens. In the design presented here, the projection lens is a plano-convex lens with a clear aperture of 30 mm. While this lens will have tight tolerances, its small size is a significant mitigating factor. This is why the condenser lens is used. Its purpose is to focus the light into the projection lens and keep this lens small. Without the condenser lens, the projection lens would be about 200 mm in diameter. This is also why the projection lens is placed inside the caustic. Trying to get the lens outside the caustic would double the size of the lens. No matter what is done to change the design, the projection lens will have to be a very high quality lens. While further analysis is required to show that placing it in the caustic is the best option, we made this choice because we wanted to keep this lens as small as possible. A final note on the projection lens is that it does not have a spacing uncertainty because the uncertainty in the distance from the projection lens to the test plate cell is given in the BLISS alignment uncertainties.

After the projection lens is the test plate cell. Within the illumination lens and test plate, the shear varies between 0.17 and 0.27 mm. This means that high spatial frequency errors will contribute to measurement error, but mid and low frequency errors will not couple strongly. Since all of the surfaces are spherical, the contribution from surface figure will be negligible. The only likely error would come from striae in the glass. This means that good quality glass is required, but it is within what is regularly manufactured. For example, if the slope of the homogeneity in the glass was 50 nm/cm RMS, this would result less than 2 nm RMS wavefront of error from both the illumination lens and test plate. If 50 nm/cm were distributed linearly over ¼ of the clear aperture of the elements, then 10 ppm homogeneity glass would be acceptable.

In addition to the tolerance on the glass quality, the small shear and spherical surfaces in the test plate cell mean that the illumination lens and convex test plate surface would not require a full aperture test. The critical figure parameter is the radius of curvature which is used to set the spacing between the BLISS and the test plate cell. We base the tolerances on experience measuring large optics with a 914 mm (36 in) spherometer. Finally, the test plate is adjusted in three degrees of freedom to null the fringes, so the location of the reference surface is controlled. The location of the element is controlled by setting the tilt on the other surface. While 50 μrad is a tight tolerance, it would result in 27 μm of runout which can be easily measured.

The last uncertainty covered in table 2 deals with the BLISS. The BLISS would be mounted almost 5 m above the test plate cell. Because errors in the alignment of the BLISS result in shear between the wavefront generated by the CGH and the secondary mirror, it is necessary to control this alignment well. The baseline plan is to use a combination of laser tracker measurements and CGH alignment marks to position the BLISS. The translational uncertainties were selected to be 0.1 mm because this is can be readily accomplished with careful laser tracker measurements. The 180 μrad clocking uncertainty comes from the angle required to generate a 0.1 mm motion of the alignment marks.

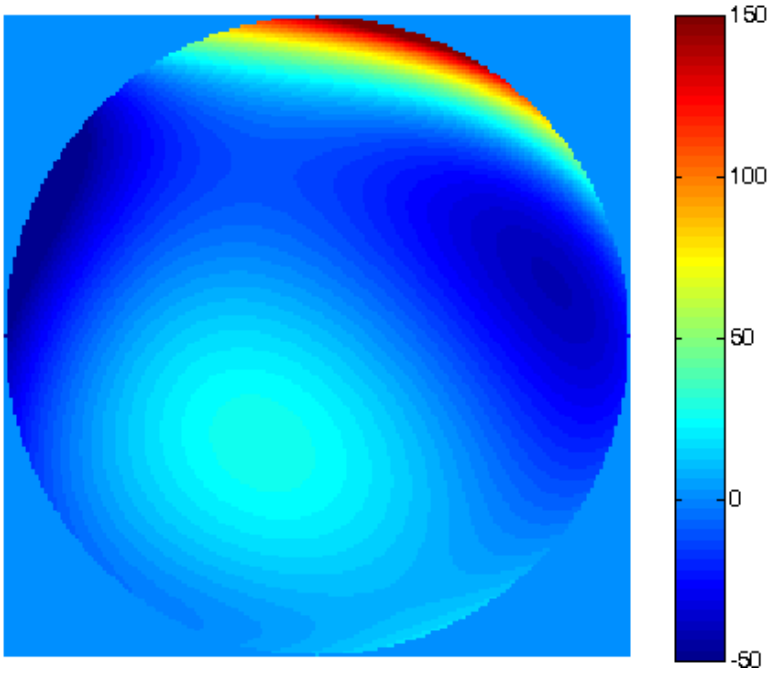


Figure 4. Errors in the interferometer due to the alignment errors and low order fabrication errors in table 2. The resulting wavefront is 28 nm RMS wavefront over a 1.1-m clear aperture.

At this point, one may ask about the tolerances in the imaging sub-system. The imaging lens is common path, so the errors that it introduces are truly insignificant. It should also be noted that the second pass through the TPC is also common path, so the errors from this sub-system are only counted once. The only potential issue with the common path optics comes from a potential ghost reflection. Because the imaging lens is in close proximity to the sensor, a ghost can be formed between the surface of the sensor and either of the imaging lens surfaces. This means that this lens requires a high performance anti-reflection coating.

Assuming that all of the uncertainties listed in table 2 are known at the 2-sigma or 95% confidence level, we have 95% confidence that the errors in the measurement of one sub-aperture will be 28.0 nm RMS wavefront. Figure 4 shows such an error. When the errors are added in quadrature for each component, the BLISS alignment errors are the leading source of error with 17.4 nm RMS wavefront. The projection lens is second with 12.9 nm wavefront. When the system errors are divided into the Zernike terms, most of the error comes from the low order terms. Z5 through Z11 account for 27.2 nm RMS wavefront while Z12 through Z43 account for 6.6 nm wavefront.

## 4. CALIBRATION

Based on our assumptions, the errors in each sub-aperture measurement will be 28 nm RMS wavefront or less (with 95% confidence). This, however, does not mean that all 28 nm of error will wind up as measurement uncertainty. Much of this error will be eliminated when the actual non-circular subaperture is used and when the surface is reconstructed based on the ensemble of subaperture measurements. Because the mirror is rotated to multiple positions, it is possible to determine that some of the data uniquely comes from errors in the interferometer. This allows one to reduce the uncertainty below 28 nm RMS wavefront.

The basic approach has been previously published[13], but a slight modification would be required for this system. For calibration, one typically moves the test optic with respect to the measurement tool in two degrees of freedom. When this is done, some contributions to the measured data can be uniquely assigned to the interferometer and some to the mirror. There is a small portion of the data that could come from either, and this is referred to as the null space.

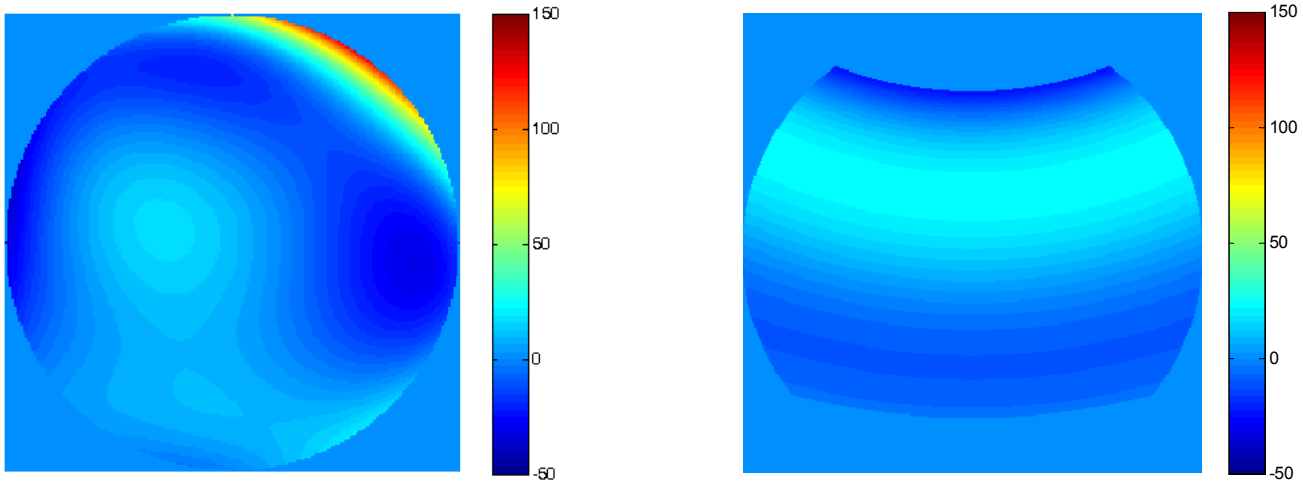


(a) (b)

Figure 5. Measurement errors divided into (a) 17.5 nm RMS wavefront non-rotationally symmetrical and (b) 13 nm RMS wavefront symmetrical errors. The non-rotationally symmetric errors can be determined using the maximum likelihood method of combining the subapertures, and do not affect the measurements. The symmetrical errors are only calculated over the clear aperture of the secondary mirror. The axis of symmetry is the axis of the secondary mirror. Units are nm.

Because the motions required for stitching in this case only require one degree of freedom, any component of the measured data that has the same axis of symmetry as the secondary mirror will be in the null space. Within the limits of noise in the system, the non-rotationally symmetrical errors will not couple into the final measurement of the mirror, but the rotationally symmetric ones can.

Figure 5 shows both of these errors. The non-rotationally symmetric terms have an RMS value of 17.5 nm RMS wavefront and the rotationally symmetrical terms contribute 13 nm RMS wavefront. When these two errors are added in quadrature, they do not produce 28 nm. This is because the rotationally symmetrical errors are only evaluated over the clear aperture of the LSST secondary mirror. When these errors are distributed over the mirror, they result in a measurement uncertainty of 13 nm RMS wavefront. Figure 6 shows the radial profile of the rotationally symmetrical errors. It is important to note that no additional processing has been done to reduce the low order errors due to the interferometer. The reduction from 28 nm to 13 nm is a benefit of the stitching process. It is also important to note that the radial errors or zones that are added to the measurement are all low order. If a third order polynomial is subtracted from the radial profile, the residual wavefront has an RMS value of 0.6 nm.

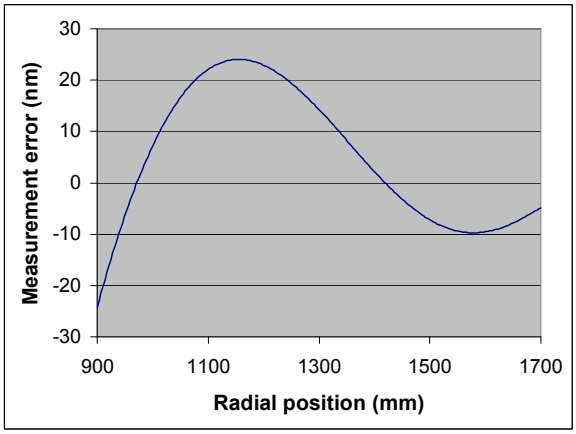


Figure 6. Radial profile of the rotationally symmetrical errors in the interferometer left after stitching. No additional correction has been applied beyond stitching.

In addition to these errors that are caused by alignment limitations, the test will have other errors from the surface irregularities and from noise. A previous analysis of a similar test showed that 3nm RMS noise in the measurements will cause ~6 nm RMS low order error in the stitched data[7].

## 5. FUTURE WORK

Up to this point, no attempt has been made to calibrate the rotationally symmetrical terms. There are several approaches for doing this. The test can be shifted radially towards the center to provide a second measurement. This would require

mechanical motion of the test and the use of a second hologram, which may be cumbersome, but would provide excellent information for resolving such errors.

It is also possible to calibrate the interferometer by testing each sub-system separately. It is possible to design a CGH that can be used to test the BLISS. A separate CGH can be used to test the TPC in the same manner as primary mirrors are tested. While this approach does not address the misalignment of the BLISS with respect to the secondary mirror, it can still be used to reduce some of the residual error.

## 6. CONCLUSION

In this paper we have presented a scalable approach for measuring large, convex surfaces. As an example, we presented a plausible system for measuring the LSST secondary mirror. Based on the sensitivity analysis, the errors due to the interferometer assembly and alignment should be less than 13 nm RMS wavefront. While this is not the only source of error, it is sufficiently low in magnitude as well as spatial frequency, that it should be acceptable for many applications. Further work is required to determine what approaches are reasonable for calibrating rotationally symmetrical errors in the interferometer as well as confirming the non-rotationally symmetrical ones. This will allow for low uncertainty measurements of the large convex surfaces that are currently being planned and the more challenging surfaces that are sure to come.

## REFERENCES


[1] Hindle, J., "A New Test for Cassegrainian and Gregorian Secondary Mirrors," Mon. Not. Royal Astron. Soc. 91, 592-3 (1931).

[2] Simpson, F., Oland, B. and Meckel, J., "Testing Convex Aspheric Lens Surfaces with a Modified Hindle Arrangement," Opt. Eng., 13(3), G101-9 (1974).

[3] Robbert, C., Yoder, P. and Montagnino, L., "Typical error budget for testing a high-performance aspheric telescope mirror," Proc. SPIE 181, 56-63 (1979).

[4] Burge, J., "Measurement of large convex aspheres," Proc. SPIE 2871, 362-373 (1996).

[5] Smith, B., Burge, J. and Martin, H., "Fabrication of large secondary mirrors for astronomical telescopes," Proc. SPIE 3134, 51-61 (1997).

[6] Spyromilio, J., "The European Extremely Large telescope: the Arne way," Proc. SPIE 6986, 05-1-8 (2008).

[7] Burge, J., Su, P. and Zhao, C., "Optical metrology for very large convex aspheres," Proc. SPIE 7018, 18-1-12 (2008).

[8] Pan, F., Burge, J., **"**Efficient Testing of Segmented Aspherical Mirrors by Use of Reference Plate and Computer-Generated Holograms. I. Theory and System Optimization," Appl. Opt., 43, 5303-5312, (2004).

[9] LSST-RefDesign.pdf

[10] Burge, J., "Fabrication of large circular diffractive optics," OSA Tech. Dig. 10, 231-3 (1998).

[11] www.4dtechnology.com

[12] www.engsynthesis.com

[13] P. Su, J.H. Burge, R. Sprowl, J. Sasian, "Maximum Likelihood Estimation as a General Method of Combining Sub-Aperture Data for Interferometric Testing**,"** Proc. SPIE 6342, X-1-6 (2006).